Identification of Bullets Based on Their Metallic Components and X-Ray Attenuation Characteristics at Different Energy Levels on CT

Dominic Gascho[1]
Niklaus Zoelch[1,2]
Henning Richter[3]
Alexander Buehlmann[4]
Philipp Wyss[4]
Sarah Schaerli[1]

[1]Department of Forensic Medicine and Imaging, Institute of Forensic Medicine, University of Zurich, Winterthurerstrasse 190/52, CH-8057 Zurich, Switzerland. Address correspondence to D. Gascho (dominic.gascho@irm.uzh.ch).

[2]Department of Psychiatry, Psychotherapy and Psychosomatics, Hospital of Psychiatry, University of Zurich, Zurich, Switzerland.

[3]Diagnostic Imaging Research Unit, Clinic for Diagnostic Imaging, Vetsuisse Faculty, University of Zurich, Switzerland.

[4]Zurich Forensic Science Institute, Zurich Canton Police and Zurich City Police, Zurich, Switzerland.

OBJECTIVE. This study aimed to identify bullets on the basis of their metallic components and to distinguish between ferromagnetic and nonferromagnetic bullets using CT.

MATERIALS AND METHODS. Eight ferromagnetic, steel-jacketed lead bullets, four nonferromagnetic, non–steel-jacketed lead bullets, and four nonferromagnetic solid bullets composed of copper or copper and zinc alloys which we refer to here as "Cu(Zn) bullets," were scanned by CT at 80, 100, 120, and 140 kVp. Attenuation values (in Hounsfield units) were measured on an extended CT scale (ECTS) in the core and at the edge of the bullets and were used to calculate the dual-energy index (DEI).

RESULTS. Although all nonferromagnetic bullets significantly differed from ferromagnetic bullets, the significant differences were solely attributed to the higher DEI of solid Cu(Zn) bullets compared with that of all-lead bullets. The lead bullets with ferromagnetic, steel-containing jackets did not differ from the lead bullets with nonferromagnetic, non–steel-containing jackets on the basis of DEIs obtained from core and edge measurements. Solid Cu(Zn) bullets could be clearly distinguished from lead bullets regardless of the metallic components of the jackets using DEI calculations from CT numbers on an ECTS. The DEIs based on the dual-energy pair 120 and 140 kVp appear to be the most appropriate for distinguishing between these two types of bullets.

CONCLUSION. This study provides new scientific knowledge regarding metals and their characteristics at different tube voltage levels. The abilities of clinically approved dual-energy CT allow differentiation of bullets composed of low-atomic-number (Z) metals from bullets composed of high-Z metals via DEI calculations from CT numbers on an ECTS.

In the United States, a weighted estimate of more than 700,000 patients with gunshot wounds presented alive at emergency departments between 2006 and 2014 [1]. Although radiography and CT are the prevalent radiologic methods used to examine patients with gunshot wounds [2], an additional MRI examination may be indicated to evaluate neurologic structures and soft tissue to document the degree of neurologic injury and detect potential infections [3, 4]. Nonetheless, in cases of gunshot injuries, MRI is rarely considered mainly because of the potential hazard that retained ferromagnetic bullet fragments may be moved or rotated in response to the magnetic torque [4, 5]. A viable noninvasive method is required to distinguish between ferromagnetic and nonferromagnetic projectiles before a patient is subjected to the magnetic field of an MRI scanner.

In 2014, Winklhofer et al. [6] presented a CT-based approach for assessing the ferromagnetic properties of ballistic projectiles in an anthropomorphic chest phantom. For distinction between ferromagnetic (steel-containing) and nonferromagnetic (non–steel-containing) projectiles, they used the dual-energy index (DEI) formula. Previously, Graser et al. [7] presented the DEI formula to reliably distinguish between different urinary stones on the basis of their components, such as pure uric acid calculi versus non–uric acid calculi. However, because the x-ray attenuation of most metallic components in projectiles is substantially greater than the x-ray attenuation of kidney stones or urinary calculi, the standard range of CT numbers is not sufficient for attenuation measurements in projectiles. This limitation can be circumvented by using the extended CT scale (ECTS) algorithm for raw data reconstruction. The ECTS algorithm was present-

TABLE 1: Characteristics of Bullets Examined for the Study

Projectile No.	Name of Manufacturer of Bullet	Bullet Brand Name or Model No.	Caliber of Bullet (mm)	Weapon	Type of Bullet	Metallic Components of Bullet[a]	
						Projectile	Jacket
1	Sellier & Bellot	.30-6 Springfield[b]	7.62 × 63	Rifle	Solid hollow point	Cu(Zn)[c]	No jacket
2	RUAG Ammotec	8 × 57 JS (RWS)[b]	8 × 57	Rifle	Semijacketed round tip	Lead	Iron or steel[d]
3	RUAG Ammotec	GP11	7.5 × 55	Rifle	Solid jacketed	Lead	Iron or steel[e]
4	RUAG Ammotec	GP90	5.56 × 45	Rifle	Solid jacketed	Lead	Iron or steel[e]
5	RUAG Ammotec	.308 Winchester (GECO)	7.82 × 51	Rifle	Solid jacketed	Lead	Iron or steel[d]
6	Prvi Partizan	.223 Remington	5.66 × 45	Rifle	Solid jacketed	Lead	Cu(Zn)[c]
7	Sellier & Bellot	0.357 Magnum	9 × 33 R	Revolver	Semijacketed hollow point	Lead	Iron or steel[d]
8	RUAG Ammotec	PP41	9 × 19	Pistol	Solid jacketed	Lead	Iron or steel[e]
9	RUAG Ammotec	7.65 Browning (MFT)	7.65 × 17	Pistol	Solid jacketed	Lead	Iron or steel[e]
10	RUAG Ammotec	6.35 Browning (GECO)	6.35 × 15.5	Pistol	Solid jacketed	Lead	Iron or steel
11	RUAG Ammotec	7.65 Browning (GECO)	7.65 × 17	Pistol	Solid jacketed	Lead	Cu(Zn)[c]
12	Prvi Partizan	9-mm Luger	9 × 19	Pistol	Solid jacketed	Lead	Cu(Zn)[c]
13	Federal Premium	Hydra-Shok	9 × 19	Pistol	Semijacketed hollow point	Lead	Cu(Zn)[c]
14	RUAG Ammotec	Action 4[f]	9 × 19	Pistol	Solid	Cu(Zn)[c]	No jacket
15	RUAG Ammotec	Swiss P[f]	9 × 19	Pistol	Solid	Cu(Zn)[c]	No jacket
16	MEN Defencetec	QD-PEP[f]	9 × 19	Pistol	Solid	Cu(Zn)[c]	No jacket

Note—Only the steel-containing bullets (projectiles 2–5 and 7–10) presented ferromagnetic characteristics, whereas projectiles 1, 14, 15, and 16 are solid bullets without a jacket.
JS and IS = Infanterie Spitzgeschoss (JS is the hunting designation), RWS = Rheinisch-Westfälischen Sprengstofffabriken, RUAG = Rüstungs Unternehmen–Aktien Gesellschaft, GP = Gewehrpatrone, GECO = Gustav Genschow & Co., R = rimmed, PP = Pistolenpatrone, MFT = Munitionsfabrik Thun, MEN = Metallwerk Elisenhütte, QD-PEP = Qick Defense–Polizei Einsatz Patrone.
[a]The metallic components were determined via collaboration with a qualified gunsmith from the Institute of Forensic Medicine and in accordance with manufacturer specifications.
[b]Hunting ammunition.
[c]The metallic component indicated as Cu(Zn) is copper or copper-zinc alloys such as tombac or brass.
[d]Tombac plated.
[e]Nickel plated.
[f]Police mission cartridge.

ed in 1990 by Klotz et al. [8] and is based on scaling down raw data by a factor of 10 before image reconstruction. These scaled-down images provide detailed depictions of metallic objects and allow measurement of CT numbers over the tenfold range [9, 10].

Winklhofer et al. [6] used ECTS reconstructions for ROI measurements. The CT numbers (the mean attenuation [in Hounsfield units]) from ROI measurements in the cores of ferromagnetic and nonferromagnetic projectiles were used to calculate the DEI for the dual-energy pairs 80/140 kVp and 100/140 kVp. Their results showed a higher mean DEI for ferromagnetic, steel-containing projectiles (80/140 kVp: mean DEI = –0.03; 100/140 kVp: mean DEI = –0.01) than that for nonferromagnetic, non–steel-containing projectiles (80/140 kVp: mean DEI = –0.07; 100/140 kVp: mean DEI = –0.06) [6]. They also measured ECTS-based CT numbers at the edges of the projectiles (presented as measurements in the jacket) but excluded them from the statistical analysis, mostly because the upper limit of the ECTS was reached.

The purpose of this study was to reproduce the results of Winklhofer et al. [6] by distinguishing between ferromagnetic and nonferromagnetic projectiles on the basis of their DEIs and to consider different projectile orientations and positions within an animal cadaver model. Furthermore, this study aimed, first, to calculate the DEI from CT numbers (on an ECTS) measured at the edge of the projectile to differentiate the metallic components of the jackets; second, to reveal the most appropriate dual-energy pair for the DEI formula to distinguish between projectiles; and, third, to assess whether there are differences in using mean or maximum attenuation values for the DEI with regard to the distinction of bullets.

Materials and Methods
Projectiles and Animal Models

Sixteen projectiles were selected for this study after consultation with investigators at the Institute of Forensic Medicine (Table 1). The projectiles were collected from shooting exercises, or the car-

tridge case was removed by means of a common kinetic bullet puller. Twelve projectiles were made of lead, eight projectiles had jackets made of steel (thus mainly iron), and four projectiles had jackets made of tombac or brass (i.e., alloys of copper and zinc). The remaining four projectiles were solid bullets (without a jacket) made of copper, tombac, or brass. Three of them were projectiles from police mission cartridges. One-half of the projectiles were ferromagnetic because they had steel-containing jackets, whereas the other half of the projectiles contained only nonferromagnetic metallic components. A simple permanent magnet was used to confirm that only the steel-containing bullets had ferromagnetic characteristics. The nonferromagnetic projectiles were additionally exposed to a 3-T MRI unit to rule out any magnetic attraction under a high magnetic field. In this article, the collective term "Cu(Zn) bullets" is used for the solid bullets made of copper or alloys of copper and zinc (projectiles 1 and 14–16 in Table 1), and the collective term "lead bullets" is used for the projectiles made of lead with jackets made of steel, tombac, or brass (projectiles 2–13 in Table 1).
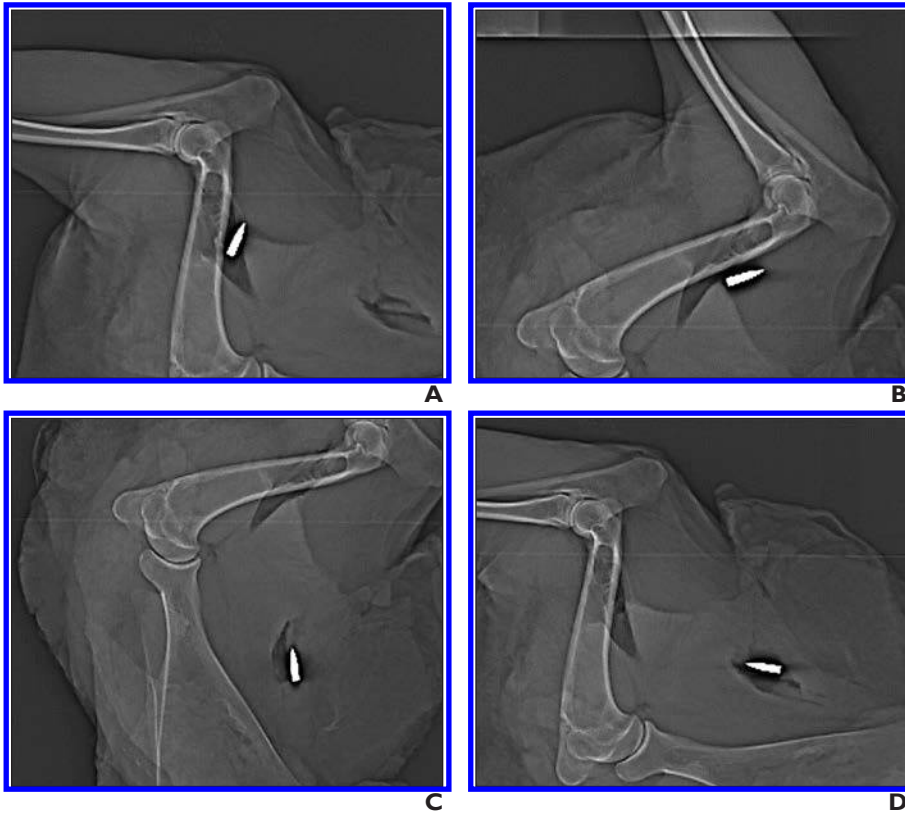
Fig. 1—Topograms of sheep cadaver leg with bullet. Each projectile was scanned at two different positions and in two different orientations.
A–D, First position was immediately adjacent to humerus inside triceps muscle (near bone, **A** and **B**), and second position was at least 5 cm from any bone inside trapezius muscle (far from bone, **C** and **D**). Each projectile was scanned in horizontal position with orientation that was parallel to z-axis of CT scanner (**A** and **C**) and with orientation that was transverse to z-axis of CT scanner (**B** and **D**); z-axis represents direction of movement of CT table through CT gantry.

The front leg of a sheep that had been severed postmortem was used as a substitute for human tissue. The sheep was euthanized for reasons unrelated to this study. The projectile was manually inserted into the muscle tissue of the front leg through a small incision, which was made with a scalpel. Each projectile was scanned at two different positions (near bone and far from bone) and in two different orientations (parallel and transverse to the z-axis of the CT scanner) (Fig. 1).

CT Data Acquisition and ROI Measurements

The projectiles were scanned by a dual-source dual-energy CT system (Somatom Definition Flash, Siemens Healthcare), which is the same CT model used by Winklhofer et al. [6]. Repeated CT scans at different energy levels were obtained using only the A tube of the CT unit. An actual dual-energy scan using the dual-source technique (thus using the A and B tubes simultaneously) does not allow selection of the ECTS algorithm for image reconstruction. Scans were obtained at four energy levels: 80, 100, 120, and 140 kVp. To achieve

the volume CT dose index of 9.8 mGy (as noted by Winklhofer et al.), the setting of 503 mAs was used for 80 kVp, 239 mAs for 100 kVp, 145 mAs for 120 kVp, and 100 mAs for 140 kVp. The data were acquired using a standard 2×64-MDCT z-flying focal spot technique. In accordance with Winklhofer et al., a slice collimation of 0.6 mm, a rotation time of 0.5 second, and a pitch of 0.6 were applied for scanning, as well as a slice thickness of 1.5 mm at an increment of 1.0 mm. The ECTS algorithm was applied for all reconstructions. The reconstruction FOV was 140×140 mm with a matrix size of 512 $\times$ 512. All reconstructions were calculated using a sharp kernel (B70) to decrease beam-hardening artifacts and partial volume effects.

CT numbers were measured after a circular ROI was drawn by use of dedicated software (MM Reading syngo.via, version VB10B HF03, Siemens Healthcare). The software enabled the same ROI position in the 80-, 100-, 120-, and 140-kVp datasets simply by means of copying and pasting the ROI. ROIs were placed at the core (ROI size, 1.6 mm^2) and at the edge (ROI size, 0.5

mm^2) of the projectile. The two ROI sizes were defined so that they fit in the core of each projectile and in the hyperdense rim at the edge of each projectile, as appropriate (Fig. 2). The mean and maximum CT numbers in Hounsfield units were measured in each ROI. If the upper limit of the ECTS was reached and the ROI indicated the maximum attenuation value of 30,710 HU, the ROI was repositioned, which means that it was shifted toward the tip of the projectile while remaining at the edge of the projectile.

A radiologic technologist (reader 1), who was blind to each projectile's components, was instructed on performing the ROI measurements. A series of measurements comprised ROI measurements of each projectile in each orientation at each position for all four energy levels in the core and at the edge of the projectile. Reader 1 performed three series of measurements in time intervals of 6 months. To determine the reproducibility of the results from ROI measurements, a second independent radiologic technologist (reader 2), who was also blind to each projectile's components, performed an additional series of measurements.

Dual-Energy Index

The DEI was calculated for the energy pairs 80 and 140 kVp (80/140 DEI), 100 and 140 kVp (100/140 DEI), and 120 and 140 kVp (120/140 DEI) according to the formula reported by Graser et al. [7], which was adapted as follows:

$$DEI = \frac{x_y - x_{140}}{x_y + x_{140} + 2000},$$

where x_y is the CT number in Hounsfield units measured at the specific energy level y ($y = 80$, 100, or 120 kVp). Accordingly, x_{140} is the CT number at 140 kVp. The DEI was calculated on the basis of the CT numbers of the mean attenuation values from the ROI measurements (DEI_{mean}), as performed by Winklhofer et al. [6]; the DEI was also calculated on the basis of the CT numbers of the maximum attenuation values from the ROI measurements (DEI_{max}).

Statistical Analysis

On the basis of the CT numbers, intraclass correlation coefficients (ICCs) were calculated to assess the intrareader agreement among the three series of measurements from reader 1 and to assess the interreader agreement between reader 2's series of measurements and reader 1's first, second, and third series of measurements. The ICCs were calculated for the CT numbers from the core and edge measurements at 80, 100, 120, and 140 kVp and were interpreted according to the guidelines of reporting ICCs described by Koo and Li [11]. The statistical tests for comparing the DEIs were select-
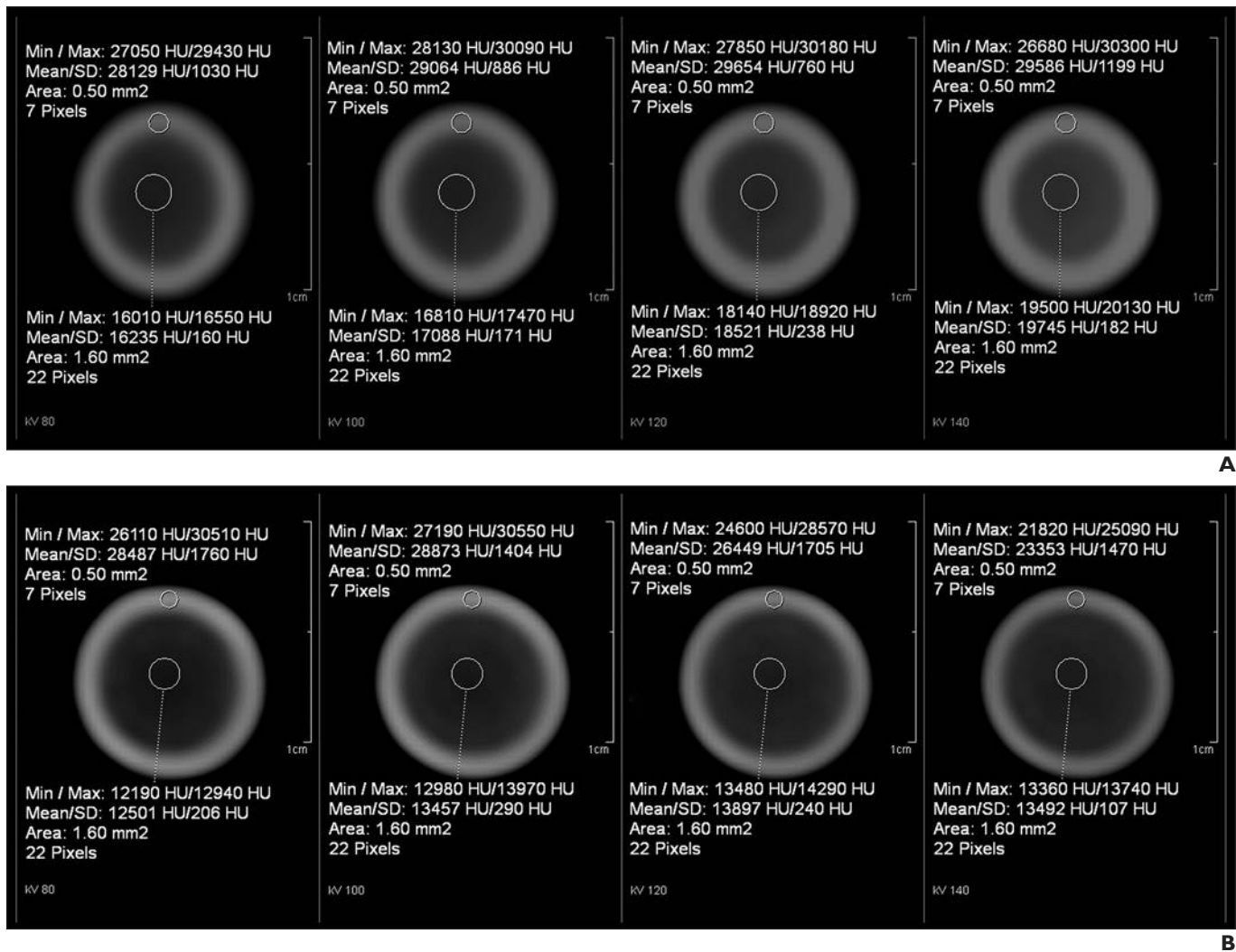
Fig. 2—CT images show attenuation measurements in ROIs at center and edge of bullets.
A and **B,** Images of lead bullet (projectile 6 in Table 1, **A**) and Cu(Zn) bullet (projectile 16 in Table 1, **B**). Projectile is clearly depicted after adjusting window settings into higher, extended range by extended CT scale (window, ≈ 40,000 HU; center, ≈ 30,000 HU). Circular ROI of 1.6 mm² in size was placed in center of projectile (*large circles*), and circular ROI of 0.5 mm² in size was placed at edge of projectile (*small circles*). Software enabled exact replication of ROI position in all tube voltage datasets. Mean and maximum (max) attenuation values were noted for each ROI measurement of each projectile and are shown above or below each ROI in each image. Note that both projectiles present with hyperdense rim even though bottom bullet is solid bullet (without jacket). Therefore, hyperdense rim does not necessarily represent jacket of projectile. Metallic component indicated as Cu(Zn) is copper or copper-zinc alloys such as tombac or brass. Min = minimum attenuation.

ed according to the results of the Shapiro-Wilk test, which determined whether the data were normally distributed. The nonparametric Mann-Whitney *U* test (two independent samples) was used to compare differences between the DEIs obtained from ferromagnetic (steel-jacketed) projectiles and the DEIs obtained from nonferromagnetic projectiles. The nonparametric Wilcoxon signed rank test (two related samples) was applied to assess differences in the DEI of each projectile according to position (near bone and far from bone), orientation (parallel and transverse to the *z*-axis), and ROI location (at the core and at the edge of the projectile). The nonparametric Kruskal-Wallis *H* test (*k* independent samples) and Dunn post hoc test with the Bon-

ferroni adjustment were used to reveal statistically significant differences among the individual projectiles. A *p* value of < 0.05 was considered statistically significant.

Results
ROI Measurements and Intrareader Agreement
Reader 1 drew 1536 ROIs (three series of measurements); thus, 768 mean attenuation values and 768 maximum attenuation values were captured for the core and edge measurements. All CT numbers were below the upper limit of the ECTS, although most of the maximum attenuation values from the edge measurements of the lead bullets were close to the

limit. Reader 1 showed excellent intrareader agreement for the core measurements (ICC, 0.92–0.95) and good intrareader agreement for the edge measurements (ICC, 0.75–0.84). All of reader 1's measurements were included in the subsequent statistical analysis.

Ferromagnetic and Nonferromagnetic Projectiles
Table 2 lists the overall mean DEI_{mean} and DEI_{max} values for all projectiles as well as for the nonferromagnetic and ferromagnetic projectiles separately. The ferromagnetic projectiles significantly differed from the nonferromagnetic projectiles. However, contrary to expectations, the DEI_{mean} and DEI_{max} of

TABLE 2: The Overall Mean Dual-Energy Index (DEI)

Dual-Energy Pairs	ROI Position	DEI Based on Attenuation (HU)	Mean DEI		
			All Projectiles	Nonferromagnetic Projectiles	Ferromagnetic Projectiles
80/140 kVp	Core	Mean	−0.068	−0.053	−0.082
100/140 kVp	Core	Mean	−0.038	−0.025	−0.051
120/140 kVp	Core	Mean	−0.014	−0.007	−0.023
80/140 kVp	Core	Maximum	−0.061	−0.042	−0.079
100/140 kVp	Core	Maximum	−0.035	−0.019	−0.050
120/140 kVp	Core	Maximum	−0.014	−0.005	−0.023
80/140 kVp	Edge	Mean	−0.012	0.013	−0.038
100/140 kVp	Edge	Mean	0.012	0.034	−0.010
120/140 kVp	Edge	Mean	0.010	0.022	−0.002
80/140 kVp	Edge	Maximum	−0.009	0.018	−0.035
100/140 kVp	Edge	Maximum	0.012	0.034	−0.011
120/140 kVp	Edge	Maximum	0.009	0.022	−0.003

Note—The overall mean DEIs of all three dual-energy pairs from the core and edge measurements were significantly higher for nonferromagnetic projectiles than those for ferromagnetic projectiles ($p < 0.01$). The overall mean DEIs obtained from edge measurements of nonferromagnetic projectiles were positive, whereas those of ferromagnetic projectiles were negative.

all three dual-energy pairs from the core and edge measurements were significantly higher for nonferromagnetic projectiles than for ferromagnetic projectiles ($p < 0.01$).

Position, Orientation, and Measurement Location

The Wilcoxon signed rank test revealed no significant differences in the DEI of projectiles located near or far from bone as determined by either edge or core mea-

surements. No significant differences were detected in the core-based DEI between the transverse and parallel projectile orientations except for the 80/140 DEI_{max} ($p = 0.038$). In contrast, at the edge, significant differences ($p \leq 0.001$) between the transverse and parallel orientations were detected for all DEIs except the 80/140 DEI_{mean}. The DEI_{mean} and DEI_{max} of all three dual-energy pairs differed significantly when

based on measurements from the core and the edge ($p < 0.001$).

Distinction Between Cu(Zn) Bullets and Lead Bullets

Among all projectiles, the Cu(Zn) bullets showed appreciably higher DEIs than the lead bullets. Table 3 provides an overview of the significant differences in the DEI between all lead bullets and each of the Cu(Zn)

TABLE 3: The Number of Significant Differences in the Dual-Energy Index (DEI) Between All Lead Bullets and Each of the Cu(Zn)[a] Bullets

Dual-Energy Pairs	ROI Position	DEI Based on Attenuation (HU)	No. of Significant Differences in the DEI Between Lead Bullets and Cu(Zn) Bullets				
			Cu(Zn) Bullets				
			Projectile 1[b]	Projectile 14[b]	Projectile 15[b]	Projectile 16[b]	Total No.
80/140 kVp	Core	Mean	4	10	11	0	25
100/140 kVp	Core	Mean	8	9	10	8	35
120/140 kVp	Core	Mean	9	10	11	9	39
80/140 kVp	Core	Maximum	5	10	11	0	26
100/140 kVp	Core	Maximum	10	10	11	8	39
120/140 kVp	Core	Maximum	9	11	11	11	42
80/140 kVp	Edge	Mean	11	5	11	10	37
100/140 kVp	Edge	Mean	11	9	11	10	41
120/140 kVp	Edge	Mean	10	10	11	10	41
80/140 kVp	Edge	Maximum	11	8	11	10	40
100/140 kVp	Edge	Maximum	11	9	11	11	42
120/140 kVp	Edge	Maximum	11	11	11	11	44

Note—The 120/140 DEI showed the most significant differences between the Cu(Zn) and lead bullets compared with the 80/140 DEI and the 100/140 DEI. The 100/140 DEI_{mean} obtained from edge measurements yielded an equal number of significant differences similar to the 120/140 DEI_{mean} obtained from edge measurements.
[a]The metallic component indicated as Cu(Zn) is copper or copper-zinc alloys such as tombac or brass.
[b]The characteristics of each projectile are listed in Table 1.
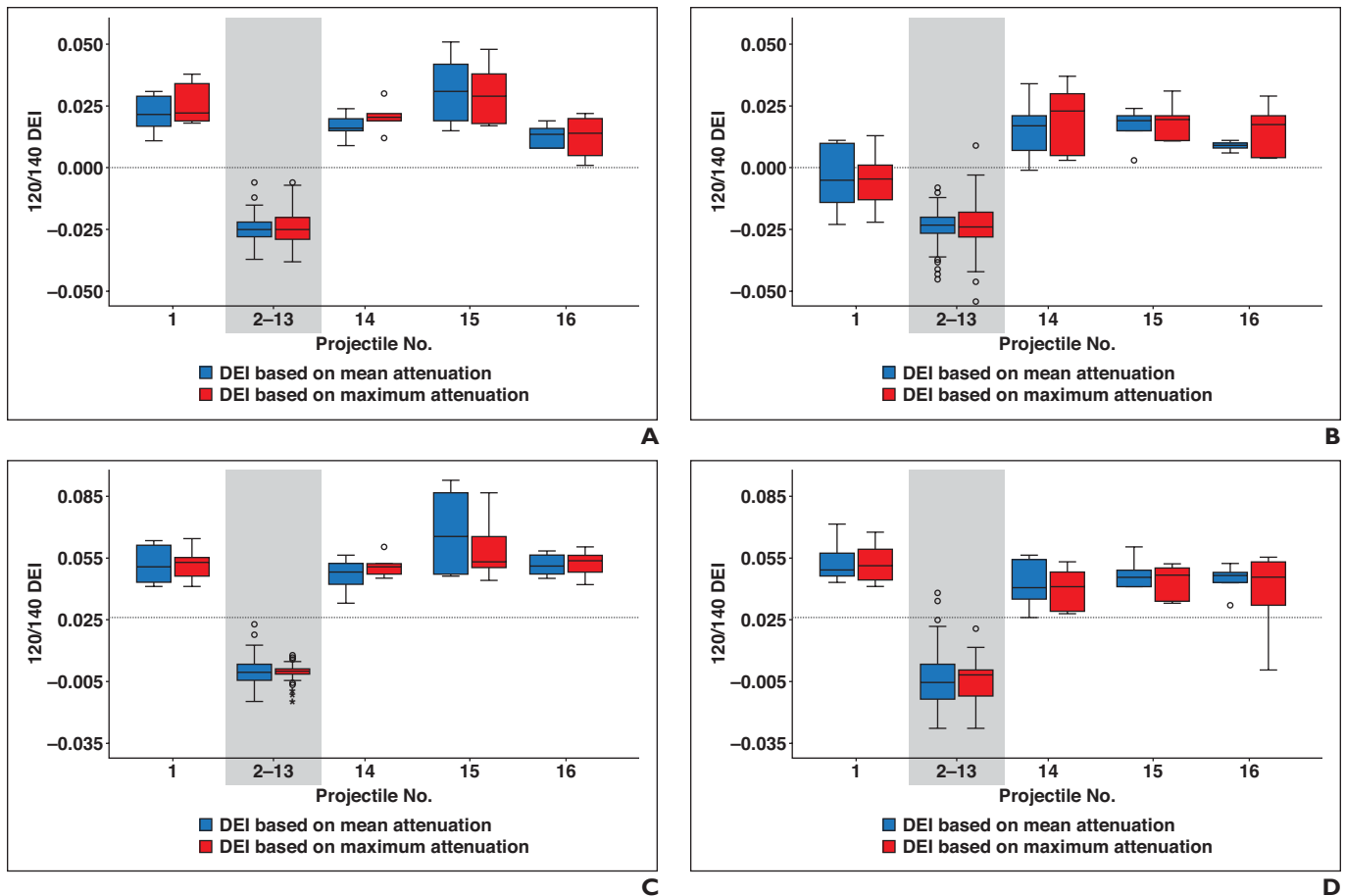
Fig. 3—Box plots show dual-energy index (DEI) values. DEI was calculated on basis of CT numbers of mean attenuation values from ROI measurements (DEI$_{mean}$); DEI was also calculated on basis of CT numbers of maximum attenuation values from ROI measurements (DEI$_{max}$). Metallic component indicated as Cu(Zn) is copper or copper-zinc alloys such as tombac or brass. Whiskers indicate minimum and maximum values; if outliers exist, whiskers represent 1.5 times interquartile range.

A and **B,** Values for 120/140 DEI$_{mean}$ and 120/140 DEI$_{max}$ from core measurements are presented with projectile in parallel (**A**) and transverse (**B**) orientation, respectively. Orientation of projectile did not impede distinction between Cu(Zn) bullets and lead bullets (*gray shading*) except for projectile 1, which presented mainly negative 120/140 DEI in transverse orientation. This projectile, hunting ammunition, had elongated shape with length of approximately 3.5 cm and long, tapered tip. Dotted lines show DEI threshold for core ROI is 0.00.

C and **D,** Similar to core measurements, 120/140 DEI$_{mean}$ and 120/140 DEI$_{max}$ from edge measurements are presented with projectile in parallel (**C**) and transverse (**D**) orientation, respectively. Apart from few outliers (*circles*), 120/140 DEIs from edge measurements were affected little by orientation of projectile. Orientation of projectile did not impede distinction between Cu(Zn) bullets and lead bullets (*gray shading*). Horizontal lines show DEI threshold for edge ROI is 0.025. In **C**, asterisks indicate extreme outliers.

bullets. The 120/140 DEI showed the most significant differences between the Cu(Zn) and lead bullets. The 120/140 DEI$_{max}$ obtained from edge measurements presented a significant difference between each of the Cu(Zn) bullets and each of the lead bullets except projectile 2. DEI thresholds (core, 0.00; edge, 0.025) were defined between the 120/140 DEI of the Cu(Zn) bullets and the 120/140 DEI of the lead bullets (Fig. 3).

Reproducibility and Interreader Agreement

Reader 2 drew 512 ROIs (one series of measurements) to reproduce the results of reader 1 with regard to distinguishing Cu(Zn) bullets from lead bullets. The interreader agreement between reader 1 and reader 2 was good to excellent for all CT numbers from mean and maximum attenuation values at the core of the projectiles (ICC, 0.76–0.95). At the edge of the projectiles, the interreader agreement was moderate to good for all CT numbers from mean and maximum attenuation values (ICC, 0.53–0.84) except for the CT numbers from mean attenuation values at 80 kVp, which presented poor agreement (ICC, 0.48).

Despite the poor agreement at the edge compared with the core, the DEIs from both measurement locations were in accordance with the respective threshold for distinguishing between Cu(Zn) bullets and lead bullets (Fig. 4).

Discussion

Although the nonferromagnetic and ferromagnetic projectiles significantly differed in terms of the mean DEI, individual comparisons among the bullets revealed no significant differences between lead bullets with ferromagnetic, steel-containing jackets and lead bullets with nonferromagnetic, non–steel-containing jackets. The significant difference between the two groups was solely attributed to the higher DEI of the solid Cu(Zn) bullets compared with all lead bullets. The presence of bone in close vicinity to the projectile did not affect the DEI. The orientation of the projectile significantly affected the DEI only when it was based on edge measurements but did not impede the differentiation between Cu(Zn) bullets and lead bullets. With regard to core-based DEIs, one Cu(Zn) bullet with an elongated shape was less clearly distinguishable from lead bullets in the transverse orientation than it was in the parallel orientation.

This study reveals four new key findings. First, solid Cu(Zn) bullets can be clearly dis-
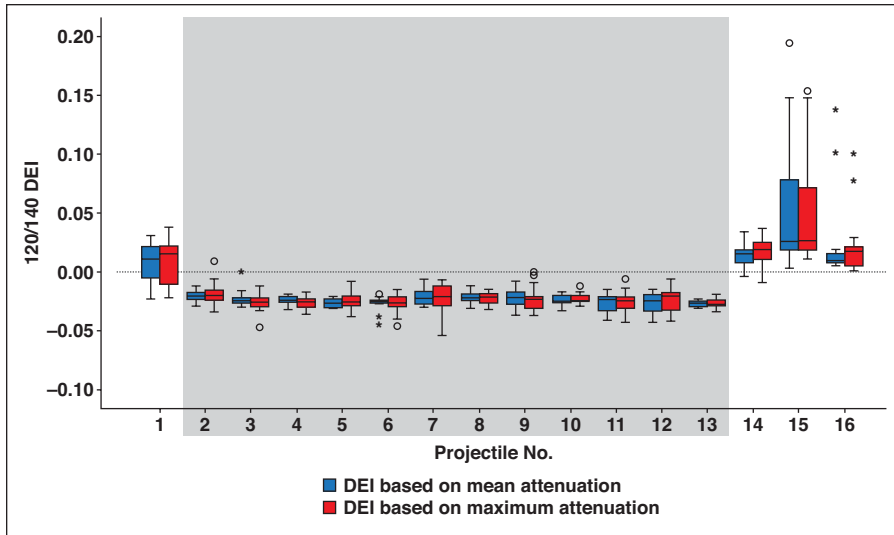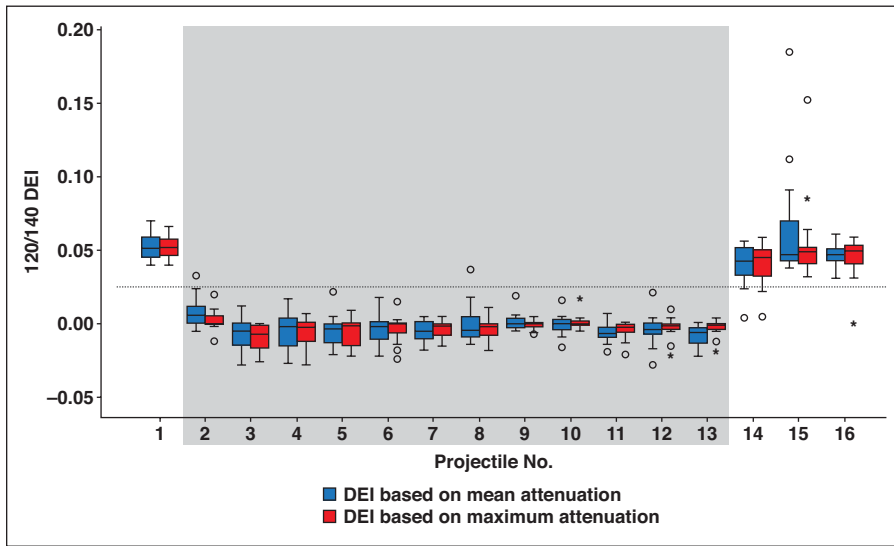
Fig. 4—Dual-energy index (DEI) was calculated on basis of CT numbers of mean attenuation values from ROI measurements (DEI$_{mean}$) and on basis of CT numbers of maximum attenuation values from ROI measurements (DEI$_{max}$). Box plots show 120/140 DEI$_{mean}$ and 120/140 DEI$_{max}$ of both readers together. Horizontal lines illustrate respective thresholds. Whiskers indicate minimum and maximum values (if outliers exist, whiskers represent 1.5 times interquartile range); circles, outliers; asterisks, extreme outliers. Metallic component indicated as Cu(Zn) is copper or copper-zinc alloys such as tombac or brass.
A, In core, DEIs of Cu(Zn) bullets were positive (apart from some negative DEIs of projectile 1), and DEIs of lead bullets (*gray shading*) were negative.
B, At edge, lead bullets (*gray shading*) show DEIs less than 0.025, whereas all Cu(Zn) bullets presented DEIs greater than 0.025. Note that projectile 1 could be clearly distinguished from lead bullets using edge-based DEIs versus core-based DEIs.

tinguished from lead bullets by means of DEI calculations from CT numbers on an ECTS. Second, edge measurements can provide usable CT numbers in the range of the ECTS, but edge-based DEIs still do not allow the differentiation of the metallic components of the jackets of lead bullets. Third, DEIs that are based on the dual-energy pair 120 and 140 kVp appear to be the most appropriate

for distinguishing between these two types of bullets. Fourth, maximum attenuation values appear more appropriate for distinguishing between Cu(Zn) bullets and lead bullets than mean attenuation values.

Winklhofer et al. [6] assumed that the presence or absence of iron or steel in the jacket was sufficient to affect the x-ray attenuation in the core and thus contribute to the

differentiation of ferromagnetic, steel-containing bullets from nonferromagnetic, non–steel-containing bullets. In contrast, the current study reveals that the DEI does not differ among lead bullets with ferromagnetic, steel-containing jackets and lead bullets with nonferromagnetic, non–steel-containing jackets. Thus, the presence of steel in the jacket does not affect the x-ray attenuation, leading to differences in the DEI between ferromagnetic, steel-jacketed and nonferromagnetic, non–steel-containing bullets, but the DEI of bullets does significantly differ according to differences in atomic number (Z) and the edge x-ray absorption of the metallic components of the core.

The DEI-based distinction between Cu(Zn) bullets and lead bullets is based on the same principle used for differentiating urinary stones or for differentiating calcification from iodine-based contrast agents [12, 13]. In the energy range of CT (< 150 keV), the x-ray attenuation of a material is characterized by scattering (Compton scatter) and absorption (photoelectric effect) [12]. Compton scatter is scarcely affected by the photon energy and is thus not decisive for material differentiation based on dual energy. In contrast, the photoelectric effect is strongly affected by the photon energy, and elements with different Z values can present certain characteristics over different energy levels related to their K-edges, which allows us to distinguish between low-Z elements such as calcium (Z = 20; K-edge = 4.0 keV) and high-Z elements such as iodine (Z = 53; K-edge = 33.2 keV) [14]. In the current study, copper (Z = 29; K-edge = 8.9 keV) and zinc (Z = 30; K-edge = 9.7 keV) were the low-Z elements, and lead (Z = 82; K-edge = 88.0 keV) was the high-Z element. The heavy metal lead showed increasing attenuation values with increasing x-ray energy, whereas copper and zinc showed their highest attenuation values mainly at 100 kVp, with decreasing attenuation values at higher x-ray energies (Fig. 5).

The difference between Cu(Zn) bullets and lead bullets at higher energies was visible not only for core-based DEIs but also for edge-based DEIs. Thus, it can be assumed that the jackets are probably too thin for the selected ROI size and that the high-Z element lead from the core mainly contributes to the CT numbers measured at the edge. Misleadingly, the ferromagnetic, steel-containing projectiles (i.e., steel-jacketed lead bullets) significantly differed from the nonferromagnetic, non–steel-containing projec-
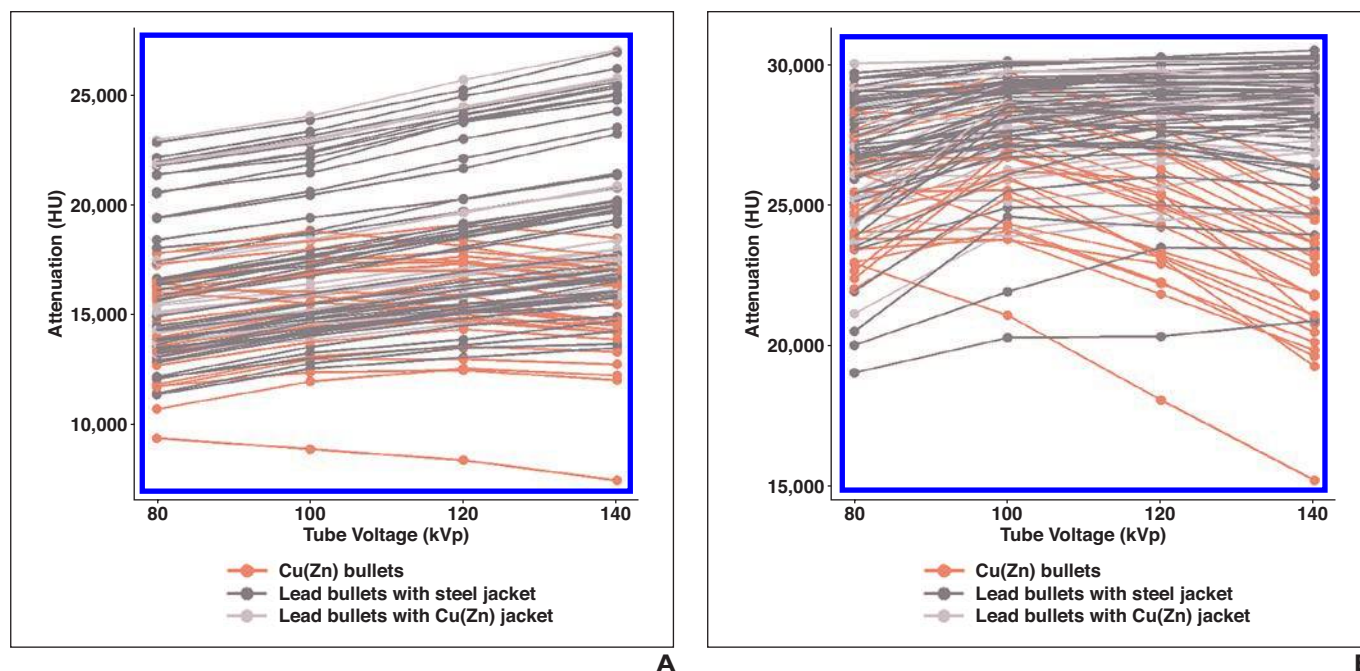
Fig. 5—CT numbers from all ROI measurements of both readers with projectiles in parallel orientation far from bone are illustrated and highlighted by connecting line to show characteristics of different types of projectiles.

A and **B,** Graphs of mean attenuation values in core (**A**) and at edge (**B**) of bullets. Lead bullets show increasing mean attenuation values with increasing tube voltage values (very pronounced in core), whereas Cu(Zn) bullets show decrease after 100 kVp (very pronounced at edge). Lead bullets presented CT numbers very close to upper limit of extended CT scale at edge of projectile. Metallic component indicated as Cu(Zn) is copper or copper-zinc alloys such as tombac or brass.

tiles—that is, from lead bullets with Cu(Zn) jackets and solid Cu(Zn) bullets. However, in the current study, the mean DEIs of nonferromagnetic projectiles were appreciably higher than the mean DEIs of ferromagnetic projectiles in contrast to the findings of Winklhofer et al. [6], who presented an inverse relationship between ferromagnetic and nonferromagnetic projectiles according to their DEIs, which were based on only core measurements. Although Winklhofer et al. also selected four solid Cu(Zn) bullets for their nonferromagnetic projectiles, their nonferromagnetic group also contained 14 lead bullets with Cu(Zn) jackets. In addition, their nine ferromagnetic projectiles comprised projectiles composed of different low-Z elements, including copper, zinc, iron ($Z = 26$), and nickel ($Z = 28$) (two projectiles contained parts of lead in their alloys) and only one (steel-jacketed) lead bullet. The large number of bullets composed of low-Z elements likely caused the higher mean DEI of their ferromagnetic projectiles, whereas the large number of bullets composed of lead ($Z = 82$) caused the lower mean DEI of their nonferromagnetic projectiles. This conjecture is supported by a comparison between the overall mean DEI of all (ferromagnetic and nonferromagnetic) projectiles in the cur-

rent study ($n = 16$; Cu(Zn) bullets, $n = 4$; lead bullets, $n = 12$) and the overall mean DEI of the nonferromagnetic projectiles reported by Winklhofer et al. ($n = 18$: Cu(Zn) bullets, $n = 4$; lead bullets, $n = 14$). The overall mean 80/140 DEI$_{mean}$ of −0.068 in the core (Table 2) is equivalent to the mean 80/140 DEI$_{mean}$ of −0.07 calculated by Winklhofer et al., and the overall mean 100/140 DEI$_{mean}$ of −0.038 in the core (Table 2) is slightly higher than the mean 100/140 DEI$_{mean}$ of −0.06 reported by Winklhofer and colleagues.

To further pursue the DEI-based distinction of ferromagnetic bullets from nonferromagnetic bullets, determining an appropriate CT protocol and attenuation measurement techniques is essential for identifying steel components in the jacket independent of the metallic components in the core. Despite the unsatisfactory results with regard to identifying ferromagnetic components in the jacket, the current study shows a new approach for identifying lead bullets noninvasively. Retained lead bullets present a potential risk for lead poisoning [15–17]. The noninvasive classification of retained bullets or bullet fragments into leaded or nonleaded bullets will lead to immediate medical clarification of potential lead poisoning in gunshot victims. Furthermore, noninvasive differen-

tiation of bullets from common ammunition and bullets from police ammunition (projectiles 14–16) is of forensic interest. Usually, bullet fragments removed from the body are submitted for quantitative compositional analysis by inductively coupled plasma atomic emission spectroscopy [18]. A comparison can then be performed with a bullet recovered at a crime scene or with bullets in a box of cartridges that is thought to have been the source of the fatal cartridge [18]. In emergency treatment, a bullet will not necessarily be removed depending on its location in the body. Using the DEI-based approach will rapidly provide information on the trace metal even before surgical procedures are performed. In a case of multiple gunshot fatalities, the DEI-based approach may rapidly provide information regarding whether more than one ammunition has been used or whether more than one shooter may be involved in the incident.

The implementation of a scan with 120 kVp (if not already used for the standard CT protocol) and a scan with 140 kVp just over the small range where a bullet is located should be considered for the CT protocol of gunshot victims for practical use of the presented method to identify the bullet on the basis of its components. A radiolo-

gist or radiologic technologist can perform the ROI measurements, and in addition to an assessment of the injuries, the radiologist can inform the police about the metallic components of the lodged bullet. Forensic pathologists, who do not have access to a CT scanner at their institutes, may cooperate with a local hospital to perform postmortem CT scans on selected cases. Several forensic institutes have established excellent relationships with nearby clinical radiology facilities and perform postmortem CT in after-hours sessions [19]. Mobile CT scanners may be helpful when several forensic institutions share a CT scanner [20].

Despite concerns of falsified results at the edge due to cupping artifacts (beam hardening) and the partial volume effect, the edge-based 120/140 DEI$_{max}$ appeared most appropriate for distinguishing between Cu(Zn) bullets and lead bullets. Because even small ROI measurements at the edge led to a clear distinction between these two types of bullets, it is promising that this approach is also viable for smaller bullet fragments. Although the orientation of the projectiles significantly affected the edge-based DEI, the threshold-based distinction between Cu(Zn) bullets and lead bullets was not impeded. However, the threshold was slightly shifted into the positive range for the 120/140 DEI values based on edge measurements compared with 120/140 DEI values based on core measurements. Therefore, the operator must be aware of the ROI position for measurement of the CT numbers that are used for calculation of the DEI. Although the dual-energy pair 120 and 140 kVp was most appropriate for distinguishing Cu(Zn) bullets from lead bullets, other dual-energy pairs may be more appropriate for differentiating between less common bullets made of other metallic components.

Some limitations of this study must be declared. First, the relative position of the projectile within the scanning field was not assessed in this study. The SD of the DEI might be increased if the projectile is located far from the isocenter of the CT gantry because of increased noise at the border of the scanning field. Second, all projectiles in this study were manually inserted into the muscle tissue. A bullet lodging inside the body after being fired will probably split into fragments or deform inside the body depending on the type of ammunition. The DEI-based assessment of the metallic components of bul-

let fragments or deformed bullets might be more challenging than for whole bullets. Additionally, several bullet fragments in close range may yield false results because of metal artifacts. Third, the DEI-based distinction of projectiles was assessed on a CT system from a single manufacturer, which does not account for interscanner variability.

In conclusion, this study provides new scientific knowledge with regard to metals and their characteristics at different tube voltage levels. The abilities of clinically approved dual-energy CT allow the differentiation of bullets made of low-Z metals from bullets made of high-Z metals via DEI calculations from CT numbers on an ECTS. Future photon-counting CT may enable differentiation of a variety of metallic elements, and together with further detector development, this method may enable differentiation between steel-containing and non–steel-containing jackets of bullets composed of lead for the triage of gunshot victims for examination by MRI.

Acknowledgments

References

1. Gani F, Sakran JV, Canner JK. Emergency department visits for firearm-related injuries in the United States, 2006–14. *Health Aff (Millwood)* 2017; 36:1729–1738
2. Reginelli A, Russo A, Maresca D, Martiniello C, Cappabianca S, Brunese L. Imaging assessment of gunshot wounds. *Semin Ultrasound CT MR* 2015; 36:57–67
3. Martinez-del-Campo E, Rangel-Castilla L, Soriano-Baron H, Theodore N. Magnetic resonance imaging in lumbar gunshot wounds: an absolute contraindication? *Neurosurg Focus* 2014; 37:E13
4. Alvis-Miranda HR, Rubiano A, Agrawal A, et al. Craniocerebral gunshot injuries; a review of the current literature. *Bull Emerg Trauma* 2016; 4:65–74
5. Wilson AJ. Gunshot injuries: what does a radiologist need to know? *RadioGraphics* 1999; 19:1358–1368

6. Winklhofer S, Stolzmann P, Meier A, et al. Added value of dual-energy computed tomography versus single-energy computed tomography in assessing ferromagnetic properties of ballistic projectiles: implications for magnetic resonance imaging of gunshot victims. *Invest Radiol* 2014; 49:431–437
7. Graser A, Johnson TR, Bader M, et al. Dual energy CT characterization of urinary calculi: initial in vitro and clinical experience. *Invest Radiol* 2008; 43:112–119
8. Klotz E, Kalender WA, Sokiransky R, Felsenberg D. Algorithms for the reduction of CT artifacts caused by metallic implants. SPIE Digital Library website. dx.doi.org/10.1117/12.18985. Published August 1, 1990. Accessed October 26, 2016
9. Gascho D, Gentile S, Bolliger SA, Thali MJ. Charon's coins. *Forensic Sci Med Pathol* 2016; 12:384–387
10. Gascho D, Thali MJ, Niemann T. Post-mortem computed tomography: technical principles and recommended parameter settings for high-resolution imaging. *Med Sci Law* 2018; 58:70–82
11. Koo TK, Li MY. A guideline of selecting and reporting intraclass correlation coefficients for reliability research. *J Chiropr Med* 2016; 15:155–163
12. Johnson TRC, Krauss B, Sedlmair M, et al. Material differentiation by dual energy CT: initial experience. *Eur Radiol* 2007; 17:1510–1517
13. Qu M, Jaramillo-Alvarez G, Ramirez-Giraldo JC, et al. Urinary stone differentiation in patients with large body size using dual-energy dual-source computed tomography. *Eur Radiol* 2013; 23:1408–1414
14. McCollough CH, Leng S, Yu L, Fletcher JG. Dual- and multi-energy CT: principles, technical approaches, and clinical applications. *Radiology* 2015; 276:637–653
15. DeMartini J, Wilson A, Powell JS, Powell CS. Lead arthropathy and systemic lead poisoning from an intraarticular bullet. *AJR* 2001; 176:1144
16. Coon T, Miller M, Shirazi F, Sullivan J. Lead toxicity in a 14-year-old female with retained bullet fragments. *Pediatrics* 2006; 117:227–230
17. Rentfrow B, Vaidya R, Elia C, Sethi A. Lead toxicity and management of gunshot wounds in the lumbar spine. *Eur Spine J* 2013; 22:2353–2357
18. DiMaio VJ. *Gunshot wounds: practical aspects of firearms, ballistics, and forensic techniques*, 2nd ed. New York, NY: Taylor & Francis, 1998
19. O'Donnell C, Woodford N. Post-mortem radiology: a new sub-speciality? *Clin Radiol* 2008; 63:1189–1194
20. Gascho D, Philipp H, Flach PM, Thali MJ, Kottner S. Standardized medical image registration for radiological identification of decedents based on paranasal sinuses. *J Forensic Leg Med* 2018; 54:96–101

This article has been cited by:

1. Arthur J. Fountain, Amanda Corey, John A. Malko, Davian Strozier, Jason W. Allen. 2021. Imaging Appearance of Ballistic Wounds Predicts Bullet Composition: Implications for MRI Safety. *American Journal of Roentgenology* **216**:2, 542-551. [Abstract] [Full Text] [PDF] [PDF Plus]